Supplementary Information: First-principles calculation of DNA looping in tethered particle experiments

Kevin B Towles, John F Beausang, Hernan G Garcia, Rob Phillips, and Philip C Nelson

Contents

S1. Notation

Here we summarize the symbols used in this paper, roughly in order of appearance. Most symbols whose use is confined to one section are not listed here.

"basepair"	when used as a length unit, $= 0.34\,\mathrm{nm}$
$k_\mathrm{B}T$	thermal energy, $= 4.07 \cdot 10^{-21}$ J at room temperature
$\rho,\ \rho_\mathrm{RMS},\ \rho_{\mathrm{RMS},t}$	projected distance from bead center to surface attachment point (Fig. 1*a*), and its averages (Sect. S3)
ℓ_helix	helical repeat length, $= (10.4\,\mathrm{basepair})$
ξ	persistence length of DNA (Sect. 3.3)
"segment," or ℓ_0	finite-element segment length, in this paper $= \ell_\mathrm{helix}/5 \approx 0.71\,\mathrm{nm}$
$L,\ L_\mathrm{loop},\ R_\mathrm{bead}$	tether length, loop length and bead radius
$\mathcal{E}$	elastic free energy cost per unit length (Sect. 3.1)
$\Delta\theta_i$	rotation angles from one segment to the next, radians (Sect. 3.1)
Ω_i	angular strain rates, radians per length (Sect. 3.1)
Q	continuum elasticity matrix (Sect. 3.1)
γ	overall normalization constant in Sect. 3.2
$\hat{\mathbf{E}}_1,\ \hat{\mathbf{E}}_2,\ \hat{\mathbf{E}}_3$	body-fixed frame vectors attached to a basepair (Fig. 2; Sect. 3.2)
$\mathsf{D},\ \mathsf{T}$	diagonalized form of Q, and its diagonalizing matrix (Sect. 3.3)
J_i	rotation generator matrices, $i = 1, 2, 3$ (Sect. 3.3)
$\mathsf{R}(k)$	rotation taking segment k to segment $k+1$ (Sect. 3.3)
$\mathsf{h}(k)$	orientation of segment k relative to space-fixed axes (Sect. 3.3)
α, β; P1,P2,A1,A2	labels specifying the four looping topologies (Sect. 5.1.2 and Fig. 5)
$P(\mathrm{looped})$	fraction of chains that are looped (Sect. 5.2, Sect. S5)
$J,\ \widetilde{J},\ \bar{J}$	J factor, differential J factor, averaged J factor (Eqns. (6, 5, 7))
ΔG_loop	free energy change of looping (Fig. 9, Sect. S5.5)
δt	shutter time, $= 30.8\,\mathrm{ms}$ in Refs. [1, 2] (Sect. S2.1)
$N_\mathrm{samp},\ N_\mathrm{eff}$	naive and effective number of independent samples in one sampling time (Sect. S3)
τ_diff	diffusion time scale (Sect. S3)
$\mathbf{M},\ \mathbf{M}^*,\ \mathbf{N},\ \mathbf{N}^*, \mathbf{M}^\mathrm{tot}$	rigid Euclidean motions characterizing LacI (Sect. S4)
K_d	equilibrium dissociation constant for operator–protein binding (Sect. S5)
$\mathrm{O}_\mathrm{id},\ \mathrm{O}_1$	ideal and wild-type operators, respectively (Sect. S5)
V	volume of an imagined container (Sect. S5.1)
$[\mathrm{LacI}]$	concentration of LacI repressor tetramers (Sect. S5)
$\delta v,\ \delta\omega$	spatial and angular tolerances for binding (Sect. S5.1)
N_gen	number of half-chains generated at a time (Sect. S6)
$N,\ M,\ K,\ K'$	counter variables (Sect. S7)

S2. Blur correction

S2.1. No-looping case

Ref. [3] used the Gaussian sampling Monte Carlo calculation outlined in Sect. 4.1 (but with a simpler elastic model for DNA) to predict successfully bead excursion for TPM data taken

with a fast ($1\,\mathrm{ms}$) shutter speed. Other experiments, however, use a longer exposure in each video frame, for example Refs. [1, 2], where the shutter is open for $30.8\,\mathrm{ms}$ (almost the entire video frame). To describe these experiments, the theory must be corrected to account for the blurring of the image due to Brownian motion of the bead during each exposure. As an extreme example, suppose the shutter were open for a time much longer than the bead's time to diffuse through its range of motion; then we would observe a blurred image centered on $\rho = 0$, but larger than the static image of the bead. In fact, some TPM implementations do study this enlarged apparent bead image [4]. In contrast, the bead-tracking method *discards* the apparent image size and instead studies the apparent bead center position as a function of time. We must now ask, how is this apparent bead center related to the true instantaneous bead position? For clarity, we will first outline a simplified form of the correction, then an improved version which we will use in Sect. 4.2 and the rest of the paper.

S2.1.1. Simple correction The image of a static bead located at $\mathbf{r}_0$ is a 2D distribution of intensity, $I_s(\mathbf{r} - \mathbf{r}_0)$, where $\mathbf{r}$ is projected position in the microscope focal plane. This distribution reflects the "actual" bead image, the microscope pointspread function, uncertainties from finite pixel size, etc. Suppose we knew that at some time t the bead's true position is $\mathbf{r}_0$. This is the quantity we want but cannot observe directly. At a later time $t+\tau$, we only know the probability distribution function (pdf) of the bead's possible positions: It's centered on a new point $\mathbf{r}_\tau$. For tethered 2D Brownian motion, and infinitesimal τ, the new distribution $P(\mathbf{r};\tau)$ is a Gaussian of width $\sqrt{2D\tau}$ centered on $\mathbf{r}_\tau = \mathbf{r}_0 + (\mathbf{f}/\zeta)\tau$ where $\mathbf{f}$ is the restoring force of the tether, $\zeta = k_\mathrm{B}T/D = 6\pi\eta R_\mathrm{bead}$ is the Stokes drag constant, and η is the viscosity of water. We can estimate the force by the Gaussian-chain approximation, $\mathbf{f} \approx -k_\mathrm{B}T\mathbf{r}_0/(L\xi)$ where ξ is the persistence length. The average expected image at time $t+\tau$ is then the convolution of the instantaneous image I_s with P. This intensity distribution is centered at $\mathbf{r}_\tau$.

We can find the average blurred image by dividing the finite (nonzero) shutter time δt into small slices $\mathrm{d}\tau$, finding the expected average image at each τ, and adding them all together. The average blurred image will be radially stretched relative to the static image, and its center will be the average of the various $\mathbf{r}_\tau$. This center will be shifted radially inward relative to the initial $\mathbf{r}_0$, so call it $S(\rho_0)\mathbf{r}_0$, where $\rho_0 = |\mathbf{r}_0|$. $S(\rho_0) < 1$ is a scale factor function that we wish to find.

In the framework of the above approximations, the center ρ_τ obeys

$$\frac{d\rho}{d\tau} = v(\rho) = -\frac{1}{6\pi\eta R_\mathrm{bead}}\frac{k_\mathrm{B}T}{L\xi}\rho. \tag{S1}$$

Let $\tau_* = 6\pi\eta R_\mathrm{bead} L\xi/k_\mathrm{B}T$. So $\rho(\tau) = \rho_0 \mathrm{e}^{-\tau/\tau_*}$. The average of this center position over a finite shutter time δt is $S(\rho_0)\rho_0$ where

$$S(\rho_0) = \frac{\tau_*}{\delta t}[1 - \mathrm{e}^{-\delta t/\tau_*}]. \tag{S2}$$

Notice that S is independent of ρ_0. For very small δt we get $S \to 1$. For large δt, we have $S \to 0$.

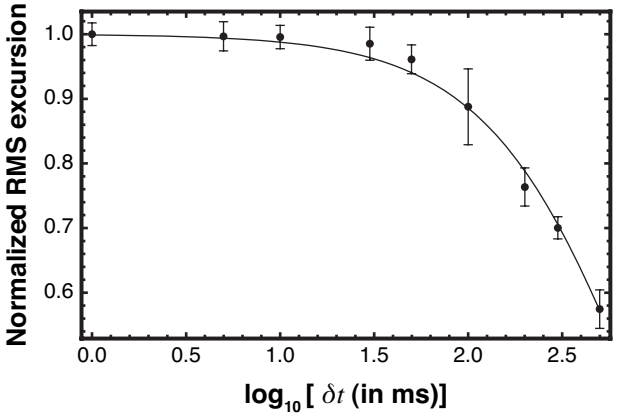

Figure S1. RMS bead excursion, $\rho_{\mathrm{RMS},\,4\,\mathrm{s}}$, as a function of camera shutter time in ms. *Dots:* Experimental data from Ref. [2]. Each dot represents about $N_{\mathrm{beads}} = 20$ different observed beads, always with an unlooped tether of length $L = 901\,\mathrm{bp}$ and a $490\,\mathrm{nm}$ diameter bead. Each such bead was observed for about $200\,\mathrm{s}$, yielding $(200\,\mathrm{s})/(4\,\mathrm{s})$ measurements of $\rho_{\mathrm{RMS},\,4\,\mathrm{s}}$, which were averaged. Each data point is the average of these N_{beads} averages; error bars represent the variation (standard deviation) among the N_{beads} beads. Each point has been normalized by the first one. The buffer used to obtain these and other experimental data in this paper was $20\,\mathrm{mM}$ Tris-acetate, pH$= 8.0$, $130\,\mathrm{mM}$ KCl, $4\,\mathrm{mM}$ $MgCl_2$, $0.1\,\mathrm{mM}$ DTT, $0.1\,\mathrm{mM}$ EDTA, $20\,\mu\mathrm{g/ml}$ acetylated BSA (Sigma-Aldrich), $80\,\mu\mathrm{g/ml}$ heparin (Sigma-Aldrich)) and $3\,\mathrm{mg/ml}$ casein (Sigma). *Curve:* Expected correction due to finite shutter speed, calculated by the method in the text (Eqn. (S2)), with $\tau_* = R_{\mathrm{bead}} L/(187\,\mathrm{nm^2 ms^{-1}})$, $R_{\mathrm{bead}} = 245\,\mathrm{nm}$, and shutter time given on the horizontal axis.

We conclude that every report of $\mathbf{r}$ is systematically too small by a factor of S, which depends on the shutter time δt and the tether length L (and other fixed quantities). If we want to predict the experimental data we should take the theoretical prediction, e.g., for ρ_{RMS}, and correct it by a factor of S. This correction is trivial to apply (it comes out of the averaging sign), because S is independent of ρ_0.

S2.1.2. Improved correction The preceding simplified discussion made some poor approximations. For example the drag constant is bigger than the naive Stokes-law formula used above, due to wall effects; also there is hydrodynamic drag on the DNA tether. Moreover, the tether end–end distance is not equal to ρ (there is also the distance from bead attachment to bead center, and foreshortening due to projection to xy plane). Nor is the tether's entropic elasticity well represented by the Gaussian-chain formula. For all these reasons, we modified Eqn. (S1), replacing $k_{\mathrm{B}}T/(6\pi\eta\xi)$ by a phenomenological parameter W_*, to be determined from experimental data (Fig. S1).

To choose an appropriate value of W_*, we simply plotted the RMS excursions for a fixed L and R_{bead} and various shutter times, normalized the values to that for very short shutter time, and fit to Eqn. (S2). Fig. S1 shows that the value $W_* = 187\,\mathrm{nm^2 ms^{-1}}$ fit the data well. We then corrected all Monte Carlo simulation results by the formula with the appropriate

L, R_{bead}, and $\delta t = 30.8\,\mathrm{ms}$. Although strictly speaking W_* is a fit parameter, its use could readily have been avoided by taking experimental data with a faster shutter speed, as was done in Ref. [3].

S2.2. Effective tether length for looped case

The blur correction described in Sect. S2.1 accounts for the finite shutter time for a tether of a length, L, assuming unbound, unlooped DNA chains. The fact that looped DNA tethers behave like much shorter, unlooped tethers, necessitates a modification to the blur correction. One could naively assume that the effective length of the tether, L_{eff}, containing a loop is just the total length of the tether minus the length of the loop, L_{loop} (i.e., $L_{\mathrm{eff}} = L - L_{\mathrm{loop}}$); however, this assumption would treat each looping topology as identical, despite their obvious differences in geometry.

We constructed a method for approximating the effective tether length based on the RMS excursion, ρ_{RMS}, of any tether type (A1, A2, P1, P2, or unlooped). Since ρ_{RMS} contains information about the geometry of the different looped topologies, it can be used to identify an effective tether length for each of the four looped topologies and the unlooped, singly-bound tether. In other words, we interpret each tether, looped or not, as behaving similarly to an unlooped, unkinked tether of length L_{eff}. The calibration curves plotted in Fig. 3 offer a convenient method for estimating values of L_{eff} for tethers of a known ρ_{RMS}. A single interpolation function of the form $\rho_{\mathrm{RMS}} = aL^b$ nicely summarizes the calibration curve for any particular persistence length; therefore, for a known RMS excursion, the effective tether length can be simply estimated as $L_{\mathrm{eff}} = (\rho_{\mathrm{RMS}}/a)^{1/b}$. Obviously, we need appropriate values of ρ_{RMS} for each tether type in order to estimate the corresponding L_{eff}. Each full tether (created as described in Sect. 6.1) is checked with multiple bead and wall boundary conditions. Tens of representative loops of each topology were used while checking tens of thousands of full tethers. For each tether type, we estimate the value of ρ_{RMS}, obtain ρ of each and calculate the root-mean-square of the entire sample. The corresponding effective tether length is then substituted into the blur correction presented in Sect. S2.1 in place of the total tether length. All results presented in Sect. 6.2 and Figs. 12 and 13 make use of this effective tether length blur correction.

S3. Simulation of sampling effects

We can see trends in the data more clearly if we reduce the distribution of bead excursions to its root-mean-square value. The question then arises of what time interval to use in the average. For a homogeneous process, like tethered motion without looping, one could in principle take a very long average, obtaining the infinite-sample RMS excursion $\rho_{\mathrm{RMS}} \equiv \sqrt{\langle\rho^2\rangle_\infty}$. If looping transitions are present but infrequent, then it makes sense to take a finite but rather long time; for example, the experiments of Refs. [1, 2] generally reported the 4-second RMS motion $\rho_{\mathrm{RMS},\,4\,\mathrm{s}} \equiv \sqrt{\langle\rho^2\rangle_{4\,\mathrm{s}}}$, or more generally $\rho_{\mathrm{RMS},t}$. Here the expectation value is limited to a sample consisting of $t/(33\,\mathrm{ms})$ consecutive video frames at a frame rate

of 30 frames per second. Note that whereas ρ_{RMS} is a single number for each bead-tether combination, in contrast $\rho_{\mathrm{RMS},t}$ has a probability distribution function. One may characterize this PDF by its mean, $\langle \rho_{\mathrm{RMS},t} \rangle_\infty$, but we must keep in mind that this quantity may not be exactly equal to ρ_{RMS}, if t is not very large.

One of our goals in this paper is to predict the distribution of $\rho_{\mathrm{RMS},t}$, as a function of bead size, tether length, and tether looping state, and of sampling time t, and to compare to experiments. To do this, we first took chains generated by our Monte Carlo algorithm and corrected each ρ value as in Sect. S2, to account for blurring. We took the resulting values in batches, found the RMS in each batch, and reported either the full probability density function of the resulting simulated $\rho_{\mathrm{RMS},t}$ values (Sect. 6.2) or its mean (Sect. 4.2). We next explain the choice of "batches" used in this procedure.

Naively one might suppose that $N_{\mathrm{samp}} = t/(33\,\mathrm{ms})$ consecutive video frames contain N_{samp} independent measurements of bead position; to simulate the RMS of those measurements, we would average the ρ^2 values from N_{samp} simulated chains. But tethered particle motion is correlated; certainly, even if we could send $t \to 0$ we should not expect to have an infinite number of independent position measurements! In fact, the diffusive autocorrelation time τ_{diff} of tethered particle motion can be measured experimentally [5–7], and typically it is longer than a video frame, particularly for long tethers and large beads. Thus the effective number of independent samples N_{eff}, will be smaller than N_{samp}.

To model this effect, we repeat a strategy used in Sect. S2.1: Estimate τ_{diff}'s scaling behavior analytically, then fix the overall normalization from one experiment. A bead in thermal motion, in a harmonic trap with stiffness κ, has a diffusive time scale given by $\tau_{\mathrm{diff}} \approx k_{\mathrm{B}}T/(D\kappa)$, where D is the bead's diffusion constant. Using the Stokes–Einstein formula for D, and the scaling relation $\kappa \approx k_{\mathrm{B}}T/L\xi$ for the spring constant of a polymer chain, gives $\tau_{\mathrm{diff}} \approx 6\pi\eta R_{\mathrm{bead}} L\xi/k_{\mathrm{B}}T$. As in Sect. S2.1, however, we expect wall effect, tether friction, etc. to make the actual drift time longer than this estimate; indeed Ref. [7] found $\tau_{\mathrm{diff}} = 140\,\mathrm{ms}$ for $L = 1000\,\mathrm{nm}$ and $R_{\mathrm{bead}} = 245\,\mathrm{nm}$. After normalizing the scaling estimate to accommodate this point, we finally took the number of effectively independent samples in a batch, to be the sampling time t (typically $4\,\mathrm{s}$), divided by the larger of $33\,\mathrm{ms}$ or our estimated τ_{diff}.

S4. Characterization of the looping synapse

In this Appendix we first discuss our mathematical treatment of O_{id} binding, then proceed to O_1. We obtained approximate geometric information about the LacI–DNA complex by applying Olson and Lu's 3DNA program [8] to Protein Data Bank entry `1LBG.pdb`. Briefly, 3DNA takes information from a PDB file, fits each DNA base to a rigid ideal, and reports the pose (position and orientation) that best represents each pair of bases.

O_{id} binding As discussed in Sect. 5.1.2, operator O_{id} can bind to a LacI dimer in either of two ways, related by a symmetry of the LacI dimer and distinguished by the label $\beta = 1, 2$. Operator O_{id} develops a large (approximately 45°) kink, localized between two of its central

basepairs, when it is bound to LacI (see Fig. 4 and Ref. [9]). We define the *entry* and *exit* basepairs as the ones located eight basepairs away from the ones straddling the kink. All basepairs between these are regarded as immobilized by binding. We found the rigid Euclidean motion $\mathbf{M}$ that carries the *entry* to the *exit* in the PDB structure, and also the rigid Euclidean motion $\mathbf{M}^*$ relating the *entry* pose to a reference frame representing the overall position and orientation of the LacI tetramer. These transformations correspond to one value for the label β. We generated a second set by exchanging the *entry* and *exit* poses, and subjecting each to 180° rotation about the $\hat{\mathbf{E}}_1$-axis.

For each choice of binding orientation β, the simulation then used $\mathbf{M}_\beta$ to join randomly generated chain segments representing the (wall)→($\mathrm{O_{id}}$ entry) and ($\mathrm{O_{id}}$ exit)→($\mathrm{O_1}$ center) DNA segments. Then the simulation examined the pose at the end of the second of these segments, as described below.

$\mathrm{O_1}$ binding: J-factor calculations Eqn. (5) expresses how we evaluate the looping J factor, by generating many chains and finding what fraction of them have the $\mathrm{O_1}$ operator close to its "target" pose for binding.‡ Here we specify the target pose. The target pose is completely determined by the pose of the DNA chain as it enters the already-bound $\mathrm{O_{id}}$, because we assume that the repressor tetramer is rigid.

The question is again complicated by the fact that binding alters the DNA, generating a kink. What, then, should we take for the optimal pose of $\mathrm{O_1}$ in an *un*bound, unkinked chain—the one that best *allows* binding? Our approach was to identify two central basepairs, namely the ones that straddle the kink in the PDB structure of a bound operator, find their two poses using 3DNA, find the rigid Euclidean motion that transforms one into the other, and apply one-half of that motion to obtain the target pose relative to the LacI tetramer, which we will call $\mathbf{N}^*$. This procedure yielded the *center* frames shown in Fig. 4; as a reasonableness check, each of these frames indeed has its $\hat{\mathbf{E}}_1$-axis directed away from the dimer, roughly along its symmetry axis. Then we generated a second target pose by rotating the first one by 180° about $\hat{\mathbf{E}}_1$; the two targets are distinguished by the value of the label $\alpha = 1, 2$ introduced in Sect. 5.1.2.

Thus our criterion for looping in configuration $\alpha\beta$ is that the central segment of $\mathrm{O_1}$ must match the entry pose of $\mathrm{O_{id}}$ transformed by $\mathbf{M}^{\mathrm{tot}}_{\alpha\beta} = (\mathbf{N}^*_\alpha)^{-1}\mathbf{M}^*_\beta$, to within some specified tolerance. A chain conformation meeting this criterion will be called "looped" when we apply Eqn. (5) to evaluate $\widetilde{J}^{(\beta)}_\alpha$.

$\mathrm{O_1}$ binding: excursion calculations Sect. 6 discusses a different calculation: Instead of just finding the probability for a loop to form, this calculation proceeds to find the probability density functions for bead location, accounting for the variety of different allowed loop states. Here it is essential to account for the kinks at *both* bound operators, because they both affect the expected bead excursion. Accordingly, whenever a chain configuration qualified as looped

‡ The loss of chain entropy as basepairs in $\mathrm{O_1}$ become immobilized is accounted for as a contribution to the binding constant K_d.

by the above criterion, we continued it beyond O_1 starting from an exit segment whose pose was related to the O_{id} entry by a rigid Euclidean motion defined analogously to $\mathbf{M}^{\mathrm{tot}}_{\alpha\beta}$ above. Once the full chain was generated in this way, and checked for steric clashes, we used its total bead displacement to build up a histogram; see Sect. 6.2.

S5. Experimental determination of looping J factor

This appendix explains how the looping J factor, defined mathematically in Eqns. (5–6), can be disentangled from the binding equilibrium constant and extracted from TPM measurements of the probability of looping $P(\mathrm{looped})$, following a simplified version of a more general treatment in Ref. [1]. Our method is similar to others in the literature [10–12], but adapted to TPM.

Our strategy is to use a "titration" method [1]. First we note that J depends only on the DNA construct used (e.g., not on the concentration $[\mathrm{LacI}]$ of free repressor protein available). However, $P(\mathrm{looped})$ depends on *both* the construct and on $[\mathrm{LacI}]$. In particular, as we increase availability of LacI, it becomes thermodynamically more favorable to bind *separate* copies of LacI to each of the two operators than to form a loop; looping is therefore suppressed at high $[\mathrm{LacI}]$ [1, 10, 11, 13]. Thus by measuring the dependence on $[\mathrm{LacI}]$, we can in principle separately determine both the binding constant K_{d} and the desired J. In practice, we will see that the available data are not yet sufficiently detailed to extract precise values for the parameters. Nevertheless, we will show how to sidestep this limitation by considering *relative* J factors.

Throughout this paper, we assume that binding of operator to LacI is equally strong in each of the two equivalent orientations (Sect. 5.1.2). And we assume that significant binding only occurs at the specific binding sites. "DNA wrapping," mediated by nonspecific electrostatic effects, is most important at very low salt concentrations, in the presence of supercoiling, and for loops of length 95–100 basepairs [14]. The first two conditions do not apply for any of the experimental data considered in the present work, and for most of our considerations neither does the last one. Moreover, others' TPM experiments apparently cannot be interpreted in terms of a wrapping-towards model of the looped conformation [15].

S5.1. Binding from solution

We first consider binding of LacI from solution to a single operator. When a molecule (e.g., LacI) binds stereospecifically to another (e.g., an operator), it must give up both translational and rotational entropy. If the first molecule was already partially constrained, both in position and orientation, then both of these entropy factors are modified. A major goal of this paper is to calculate such effects precisely. As a start, this subsection will establish some notation for the unconstrained binding process.

Each of the two constituent dimers of LacI has a binding site. Although DNA binding is probably a multi-step process, involving sequential contacts between two "heads" on a dimer with DNA regions straddling the center of the operator [9], nevertheless for our purposes we

will further idealize binding as a one-step process.§

For illustration, we begin by imagining an isolated operator segment of DNA, immobilized in a box of volume V containing solvent and a *single LacI tetramer*. Later we will remove this artificial constraint.

Each of the binding sites defines a "target pose," that is, a specific position in space where the center of the operator must lie, and a specific spatial orientation that the operator must assume, in order for binding to be possible in an encounter between the binding site and the operator. We divide the states of the LacI–operator system into two classes:

(a) The subset of states for which the LacI tetramer is positioned such that the operator is close to one of the two target poses for one of the two binding sites (to within a tolerance $\delta v \delta\omega$; see Sect. 5.2).

(b) All other positions and orientations of LacI.

We implement "binding" in the partition sum by rewarding states in class ***a*** with an extra statistical weight factor $\mathcal{W} = 8\pi^2(4K_\mathrm{d}\delta v\delta\omega)^{-1}$. Here K_d is a constant with dimensions of volume^{-1}, that is, concentration. The peculiar and arbitrary-looking form of this factor will prove convenient later; in any case it introduces an unknown constant K_d that describes the strength of binding.‖

The prescription in the preceding paragraph seems to depend on three parameters: $K_\mathrm{d},\ \delta v$, and $\delta\omega$. In practice, simple binding is described by a single equilibrium constant; we cannot experimentally determine independent values for all three parameters. But the prescription has been arranged so that the limit $\delta v \to 0, \delta\omega \to 0$ exists; in this limit a single constant K_d indeed describes the model. We will proceed using this limit. In our numerical work δv and $\delta\omega$ will take finite values, but we checked that they are small enough to give reasonable estimates of the limiting behavior (Sect. 5.3.2). As mentioned in Sect. 5.2, the normalization of $\delta\omega$ is defined such that the total volume of the rotation group is $8\pi^2$.

The partition sum Z involves an integral over all positions $\mathbf{r}$ and orientations ω of the repressor tetramer (recall that we assumed that the operator was immobilized). There are four different possibilities for binding: Either of the two binding sites may bind to the operator in either of its two equivalent target orientations. Thus we have

$$Z = \left[\mathcal{W}\int_{\boldsymbol{a}\text{ states}} \mathrm{d}^3\mathbf{r}\mathrm{d}^3\omega\right] + \left[\int_{\boldsymbol{b}\text{ states}} \mathrm{d}^3\mathbf{r}\mathrm{d}^3\omega\right]. \tag{S3}$$

The first integral equals the volume of the target, or $\delta v\delta\omega$, times 4 (the number of different allowed binding configurations). The second integral covers essentially all of space and all orientations, so $Z \approx (4 \times 8\pi^2/4K_\mathrm{d}) + 8\pi^2 V$.

Let ψ be the indicator function for binding, i.e. $\psi = 1$ on ***a*** states and 0 otherwise. The probability of being bound is thus $\langle\psi\rangle = 4{\times}8\pi^2/(4K_\mathrm{d}Z) = V^{-1}/(V^{-1} + K_\mathrm{d})$. (The initial definition of the weighting factor $\mathcal{W}$ was arranged to make this formula simple.)

We assumed that there was just one LacI in the box, so $V^{-1} = [\mathrm{LacI}]$. So

$$\frac{P(\mathrm{bound})}{P(\mathrm{unbound})} = \frac{[\mathrm{LacI}]}{[\mathrm{LacI}] + K_\mathrm{d}}\frac{[\mathrm{LacI}] + K_\mathrm{d}}{K_\mathrm{d}} = \frac{[\mathrm{LacI}]}{K_\mathrm{d}} \quad \text{(binding from solution)}. \tag{S4}$$

§ Because we treat binding in exactly the same way in this subsection and the next, any error we make from this idealization should cancel in our determination of the J factor.

‖ Equivalently, one can regard the quantity $-k_\mathrm{B}T\ln\mathcal{W}$ as a "binding free energy change," which however depends on a choice of "lattice cell size" $\delta v\delta\omega$.

Thus our prescription agrees with the usual definition of the dissociation constant [16]. The virtue of formulating the standard result in this somewhat elaborate way will become apparent in the following subsection, where we incorporate looping effects.

If the operator is not isolated and immobilized, but instead is part of a long DNA and free in solution, everything above is unchanged. The many conformations of the long DNA are irrelevant. Similarly, if there are many copies of LacI, in a container of infinite volume, again nothing changes: Only the concentration $[\mathrm{LacI}]$ enters Eqn. (S4).

S5.2. The looping J factor

Next we suppose that the operator of interest is part of a long DNA, and that there is a second operator, located elsewhere on the same long DNA.

As discussed in Sect. 5.1.1, we will simplify the analysis by assuming that a LacI tetramer is always bound to the second operator; then loop formation involves binding that same tetramer to the first one. In the system we study, the second operator is $\mathrm{O_{id}}$, which binds more strongly than the first ($\mathrm{O_1}$).¶ This simplifying assumption can be removed; see the more detailed discussion in Ref. [1]. Sect. 5.1.2 introduced the label β to indicate the binding orientation of LacI on the second operator (see also Fig. 5).

The J factor defined in Eqn. (5) quantifies how much binding to $\mathrm{O_1}$ is affected by its physical attachment to $\mathrm{O_{id}}$ via the intervening DNA. For example, this tethering maintains an effective concentration of LacI binding site in the neighborhood of $\mathrm{O_1}$, regardless how low the general LacI concentration may be. More subtly, the tethering may imply that, if a chance fluctuation brings the $\mathrm{O_1}$ close to the bound LacI's target position, it is likely to have one particular orientation. Then the probability of binding will depend on whether that preferred orientation coincides with the target orientation imposed by the geometry of LacI (see Fig. 6). Our simulations account for this effect, and quantify it (Sect. 5.3.1).

As in Sect. S5.1, we again begin by assuming that there is *exactly one* other LacI tetramer (besides the one permanently bound to $\mathrm{O_{id}}$), then later remove this assumption. The second tetramer may either be free in solution or bound to $\mathrm{O_1}$. Hence we have a competition: $\mathrm{O_1}$ can bind nothing, the second LacI previously in solution, or the LacI already bound to $\mathrm{O_{id}}$ (thus forming a loop). So the division of states in Sect. S5.1 becomes slightly more complicated, including now [4, 12, 13, 15]:

($\boldsymbol{a}_1$) $\mathrm{O_1}$ is in the target for binding to the already-bound LacI, forming a loop; the second LacI is free in solution;

($\boldsymbol{a}_2$) $\mathrm{O_1}$ is in the target for binding to the second LacI (no loop);

(b) $\mathrm{O_1}$ is unoccupied and the second LacI is free (no loop).

For a given orientation β at $\mathrm{O_{id}}$, the looped states $\boldsymbol{a}_1$ divide into two distinct topologies labeled by α (see Fig. 5). The unlooped state $\boldsymbol{a}_2$ has four possible realizations, as in Sect. S5.1.

With the terminology established, we can now symbolically express the full partition sum. As before, let $\mathbf{r}, \omega$ be the position and orientation of the second LacI tetramer. Let Z_{chain} be the partition sum for chain conformations. Thus the part of Z_{chain} attributable to looped

¶ Ref. [12] made a similar approximation to ours. In the case where the two operators are identical, the formulas are slightly different [13].

chains in the class α, β is $\widetilde{J}_\alpha^{(\beta)} \delta v \delta\omega Z_{\rm chain}$. We implement binding at O_1 as before, so the partition sum for a given β is now

$$\begin{aligned} Z^{(\beta)} &= Z^{(\beta)}_{\boldsymbol{a}_2} + Z^{(\beta)}_{\boldsymbol{b}} + Z^{(\beta)}_{\boldsymbol{a}_1} \\ &= Z_{\rm chain}\left(\left[\frac{4\times 8\pi^2}{4K_{\rm d}\delta v\delta\omega}\delta v\delta\omega\right] + 8\pi^2 V\left[1+\frac{8\pi^2}{4K_{\rm d}\delta v\delta\omega}(\widetilde{J}_1^{(\beta)}+\widetilde{J}_2^{(\beta)})\delta v\delta\omega)\right]\right) \\ &= Z_{\rm chain} 8\pi^2 (K_{\rm d}^{-1} + V + V(8\pi^2/4K_{\rm d})(\widetilde{J}_1^{(\beta)}+\widetilde{J}_2^{(\beta)})). \end{aligned} \tag{S5}$$

β is usually fixed as the loop forms and breaks, but from time to time changes as LacI unbinds and then quickly rebinds to $\mathrm{O}_{\rm id}$. Summing over the two binding orientations at $\mathrm{O}_{\rm id}$, $\beta = 1, 2$, gives

$$Z_{\rm tot} = Z_{\rm chain} 8\pi^2 \Big(2K_{\rm d}^{-1} + 2V + V 8\pi^2 (4K_{\rm d})^{-1} (\textstyle\sum_{\alpha,\beta} \widetilde{J}_\alpha^{(\beta)})\Big). \tag{S6}$$

This time we find

$$\frac{P(\text{unlooped})}{P(\text{looped})} = \frac{2K_{\rm d}^{-1}+2V}{(V8\pi^2/4K_{\rm d})(\sum_{\alpha,\beta}\widetilde{J}_\alpha^{(\beta)})} = 2\frac{V^{-1}+K_{\rm d}}{8\pi^2\widetilde{J}_{\rm tot}} = 2\frac{[\mathrm{LacI}]+K_{\rm d}}{J}. \tag{S7}$$

Above we used the abbreviations introduced in Eqn. (6). For very long loops, for which the distribution of operator orientations is isotropic, our quantity J indeed reduces to the traditional looping J factor. As in Sect. S5.1, Eqn. (S7) is also valid when there are many copies of LacI, in infinite volume.

The experiments of Ref. [1] measure the LHS of Eqn. (S7) as a function of $[\mathrm{LacI}]$, so for each DNA construct we can in principle find the slope and intercept to extract both $K_{\rm d}$ and J (see Fig. S2).

S5.3. Alternate LacI conformations

Early structural work noted that the "V-shaped" form of the LacI tetramer might not be its only conformation [9,17]. Later, electron microscopy [18] and solution studies [19] seemed to show that indeed an alternate ("open" or "extended") conformation was prevalent. Recently, TPM experiments found evidence for multiple looped states [1,15,20], which were sometimes interpreted as evidence for an open conformation [15,20]. Theoretical analyses have assumed a two-state character to the equilibrium between these forms, variously estimating the free energy cost to switch to the extended conformation as about $0\,k_{\rm B}T$ [21], 1.8–$9.4\,k_{\rm B}T$ [22], or $7k_{\rm B}T$ [15]. But all-atom simulation of DNA complexed to LacI shows no sign of any opening of the V-form [23]. Indeed, Villa et al. found flexibility in the head (DNA-binding domains), but a "locking" mechanism maintaining the overall V-form even in the presence of significant external stress.

To address this issue, in the present work we have chosen to include *only* the V-form of the tetramer. Flexibility in the binding heads can be incorporated via the tolerances $\delta v, \delta\omega$ introduced in Sect. 5.2. Sect. 6.2 shows that this picture suffices to explain in some detail much of the TPM data in Ref. [1]. In particular, the presence of three peaks in the distribution of bead excursions [1, 15, 20] emerges naturally from our analysis, without requiring that we

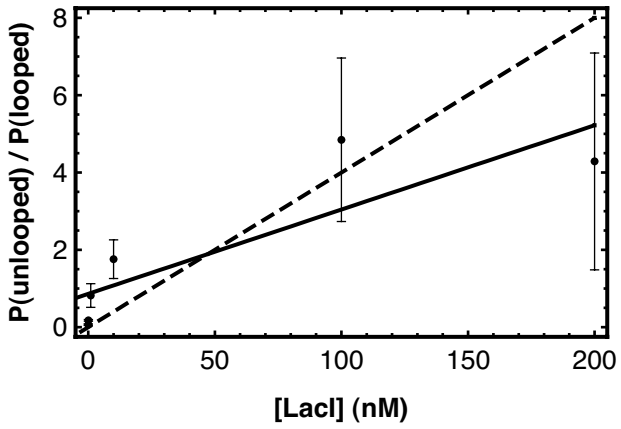

Figure S2. Determination of the looping J factor by titration. *Dots:* experimental values for the ratio $P(\mathrm{unlooped})/P(\mathrm{looped})$, for $L_{\mathrm{loop}} = 306\,\mathrm{bp}$ (from [1]). The lines represent the formula Eqn. (S7), with two different sets of parameters. Although these data do not determine the binding constant K_{d} well, nevertheless the looping J factor roughly lies between $92\,\mathrm{nM}$ (*solid line*) and $50\,\mathrm{nM}$ (*dashed line*).

postulate any extended conformation. Nevertheless, we cannot rule out such states, and Wong et al. have argued that they are necessary to explain the direct transitions they see between the different looped-state peaks. Accordingly, we now briefly indicate how to incorporate them into the analysis of the previous subsection.

We suppose that there exists an alternate conformation of LacI, with a different "target" for binding operator DNA, and that it costs free energy ΔG to switch into this conformation. Now we have two additional J-factors $\widetilde{J}_3^{(\beta)},\ \widetilde{J}_4^{(\beta)}$, and

$$Z^{(\beta)} = Z_{\mathrm{chain}} 8\pi^2 (K_{\mathrm{d}}^{-1} + V + (V 8\pi^2/4K_{\mathrm{d}})(\widetilde{J}_1^{(\beta)} + \widetilde{J}_2^{(\beta)} + (\widetilde{J}_3^{(\beta)} + \widetilde{J}_4^{(\beta)})\mathrm{e}^{-\Delta G}/k_{\mathrm{B}}T))$$

from which we can get a generalization of Eqn. (S7).

S5.4. J factor from TPM data

Han et al. measured the probability of looping, $P(\mathrm{looped})$, for the $I = 6\,\mathrm{bp}$, "long" construct, as a function of $[\mathrm{LacI}]$ [1]. This construct has $L_{\mathrm{loop}} = 306\,\mathrm{bp}$ (see Eqn. (4)). More precisely, Han et al. made a histogram of RMS bead displacement over 4-second windows, identified one peak corresponding to unlooped DNA tethers, and compared the area under that peak to the area under the other peaks, with results shown in Fig. S2.[+] The trend roughly resembles the prediction in Eqn. (S7), with J factor in the range 50–$92\,\mathrm{nM}$. We will call this (still rather imprecisely determined) quantity J_*. More extensive future measurements of this type could yield a more precise estimate of the slope, and hence a better value for J_* (and also J at other loop lengths).

[+] The data shown in the figure correspond to a concentration regime where the stronger operator $\mathrm{O_{id}}$ is essentially always bound to repressor. At lower $[\mathrm{LacI}]$ than shown here, looping is suppressed, and the curve in Fig. S2 bends upward, as the occupancy of the strong operator ($\mathrm{O_{id}}$) decreases [1].

Pending the availability of such data, we note another consequence of Eqn. (S7): The binding constant K_d is independent of the details of the DNA construct. Thus, if we have measurements of $P(\mathrm{looped})$ at two different loop lengths with the same $[\mathrm{LacI}]$, then we can use that information to extract the *relative* J factor:

$$\frac{J(1)}{J(2)} = \frac{P(\mathrm{unlooped}, 2)}{P(\mathrm{looped}, 2)} \frac{P(\mathrm{looped}, 1)}{P(\mathrm{unlooped}, 1)}. \tag{S8}$$

Han et al. only obtained the full titration curve for one particular loop length; at all other loop lengths they held $[\mathrm{LacI}] = 100\,\mathrm{pM}$. Nevertheless, by using Eqn. (S8) we can find J factors at the other loop lengths as

$$J(L_\mathrm{loop}) = J_* \frac{P(\mathrm{unlooped}, *)}{P(\mathrm{looped}, *)} \frac{P(\mathrm{looped}, L_\mathrm{loop}, 100\,\mathrm{pM})}{P(\mathrm{unlooped}, L_\mathrm{loop}, 100\,\mathrm{pM})}. \tag{S9}$$

In this expression $*$ refers to $L_\mathrm{loop} = 306\,\mathrm{bp}$ and $[\mathrm{LacI}] = 100\,\mathrm{pM}$. Sect. 5.4 uses this relation to compare our predictions to existing experiments.

S5.5. J factor from in vivo data

Eqn. (S6) with Eqn. (6) gives the relative contributions of the classes of states as $Z_{\boldsymbol{b}} : Z_{\boldsymbol{a}_1} : Z_{\boldsymbol{a}_2} = 1 : \frac{J}{2K_\mathrm{d}} : \frac{[\mathrm{LacI}]}{K_\mathrm{d}}$. In the language of Ref. [12], these ratios appear as $1 : \mathrm{e}^{-(\Delta G_{\mathrm{O}_1} - \Delta G_\mathrm{loop})/k_\mathrm{B}T} : ([\mathrm{LacI}]/1\,\mathrm{M})\mathrm{e}^{-\Delta G_{\mathrm{O}_1}/k_\mathrm{B}T}$. Comparing shows that $K_\mathrm{d} = (1\,\mathrm{M})\mathrm{e}^{\Delta G_{\mathrm{O}_1}/k_\mathrm{B}T}$ and $-\ln[J/(1\,\mathrm{M})] = \Delta G_\mathrm{loop} - \ln 2$. Following the discussion and notation of Ref. [12], we thus have

$$J = 2[\mathrm{LacI}] \left(\frac{R_\mathrm{loop} - R_\mathrm{noloop}}{R_\mathrm{noloop} - 1} \right). \tag{S10}$$

The dots in our Fig. 10 show this formula, applied to experimental data of Ref. [24] and assuming that $[\mathrm{LacI}] = 75\,\mathrm{nM}$ [12, 24]. We caution, however, that our simulation results cannot be directly compared to *in vivo* data, as the experimental conditions are quite different in the two cases.

S6. Alexandrowicz chain generation

Chains were generated using a short-cut method proposed by Alexandrowicz [25,26]. Briefly, instead of generating entire chains, sets of N_gen half-chains of length $L_\mathrm{loop}/2$ were generated; pairs of half-chains were then selected and joined end-to-end to produce N_gen^2 whole chains of length L_loop. Although this method sacrifices some independence between elements of the generated chains, steps were taken to minimize this effect while maintaining a significant computational speed-up. The sample size, N_gen, was kept at or below 10^3, meaning each time 10^3 half-chains were generated, 10^6 full chains were tested. Since typical simulations tested on the order of 10^{10} chains, sample set generation was done on the order of 10^4 times. The Alexandrowicz method was validated by comparing a subset of the results against those of chain generation by using a non-Alexandrowicz method (i.e., full-chain generation rather than half-chain generation) (data not shown).

S7. Monte Carlo algorithms

In order to increase further the efficiency of our sampling method, all four looping topologies were tested in parallel for each generated chain; moreover, several $L_{\rm loop}$ values were tested for each generated chain. We chose to test loop lengths over three helical repeats of DNA, equivalent to a range of 15 of our segments. In order to accomplish this without introducing bias into our half-chain generation method, truncated chains were generated by removing one segment from alternating ends of the whole generated chain. For example, suppose we wish to test chains from 35–50 segments per loop. First, we generate a sample of $N_{\rm gen}$ half-chains of length 25 segments. We choose two of these and join them to make a whole chain with segments numbered 1 through 50, and test it for looping, in all four possible binding configurations $(\alpha,\beta) = (11),\ (12),\ (21),\ (22)$. Then we remove segment 50 and test again for looping (49 segment loop length), then remove segment 1 and test again (48 segment loop length), and so on. In this way, each generated chain actually yielded contributions to 60 different calculated quantities.

Looping, as defined by our method, is a rare event, especially for short loop lengths (about one in every 10^8 chains meets the looping criteria). Accordingly, we introduced a method for splitting the problem into two separate parts, which we refer to as the N/K and M/K' algorithms (summarized in Fig. S3).

N/K algorithm First, we generate only the loop (interoperator) section of the tether, to avoid wasted computation time on the wall-to-loop and loop-to-bead segments. As described in Sect. S6, we use the Alexandrowicz method; thus we first generate $N_{\rm gen}$ half-chains. Creating one whole chain from two chosen half-chains, we then test the chain against the looping criteria described in Sect. 5.3.2 and Sect. S4. If it passes, we declare it to be "looped" and proceed; otherwise we increment K and choose a new pair of half-chains and repeat. For the few interoperator chains that do pass, we then generate the remaining wall→($\rm O_{id}$ entry), and $\rm O_1$→bead segments of the chain.

Finally, for every complete chain generated in this way we must also choose random orientations for the starting end of the chain relative to the wall. Only after choosing a chain–wall orientation can we rotate every chain segment rigidly into its proper position relative to the wall and check whether any segment collides with the wall. Similarly, a choice of chain–bead orientation is needed before we can check whether any chain segment, or the wall, collides with the bead. For each complete generated chain we drew 1000 different pairs of end orientations to check for steric clashes.

If the complete chain, wall, and bead satisfy all the steric constraints (no bead–chain, bead–wall, or wall–chain overlap), we call the conformation "looped and allowed" and increment N. In any case, we increment K. Once we repeat this process for the generated set of $(N_{\rm gen})^2$ half-chains, we generate a new set and repeat. The resulting ratio N/K gives the number of "looped and allowed" conformations, relative to the total number of tested chains. But this ratio is not quite the quantity $\tilde{J}$ defined by Eqn. (5), because not all of the chains tested would have given rise to allowed conformations.

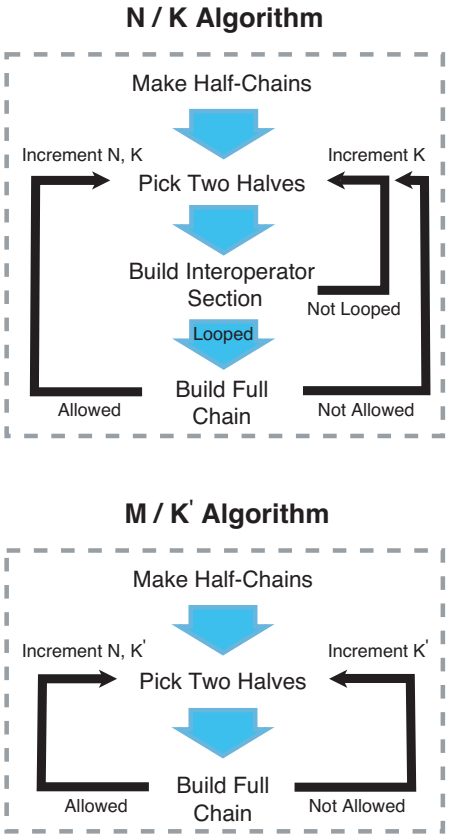

Figure S3. Summary of N/K and M/K' algorithms. Each dashed box corresponds to the algorithm for a single set of N_{gen} half-chains. The chains are combined end-to-end to form N_{gen} whole chains. Each of these whole chains is tested to assess looping and/or steric constraints depending on the algorithm being used. The resulting ratios produced by each algorithm lead to a value for the differential J factor via Eqn. (5).

M/K' algorithm In principle, we could extend *every* generated interoperator chain to a full chain conformation, by always appending wall$\rightarrow \mathrm{O}_{\mathrm{id}}$ and $\mathrm{O}_1 \rightarrow$bead segments and wall–chain and chain–bead orientations. Then we could count the number M that are allowed, and compute N/M, the quantity needed in Eqn. (5). In practice, this procedure would wastefully generate many more complete conformations than are actually needed. Instead, we did a separate side calculation of M/K'. This algorithm is very similar to the N/K algorithm, except that we do not check for looping. Again we choose two half-chains for the interoperator region, plus the two flanking chains and orientations at the bead- and wall-ends. This time, however, we only test whether each built chain is allowed (i.e., it passes all steric constraints). If it is allowed, we increment M; in any case we increment K'. The resulting ratio of M/K' gives the number of "allowed" chains relative to the total number of tested chains; it requires testing many fewer chains than the full N/K algorithm.

Combining the ratios from the two algorithms, $(N/K) \times (M/K')^{-1}$, yields the ratio of "looped and allowed" chains to total "allowed" chains, corresponding to the fraction in the looped state; this quantity lets us calculate $\widetilde{J}_{\alpha}^{(\beta)}$ in Eqn. (5), and hence the J factor via Eqn. (6).

S8. Two alternative elastic models

S8.1. Comparison to isotropic elasticity model

The results of the isotropic elasticity model were remarkably similar to the those of the anisotropic model (data not shown). To compare the isotropic model properly to the anisotropic model used in the main text, we again followed the procedure of Sect. 3.3 to give the former the same persistence length as that used for the latter. This procedure, and a representative choice for the ratio of twist to bend stiffnesses, yielded the elasticity matrix $\mathsf{Q} = \left[\begin{smallmatrix} 44 & 0 & 0 \\ 0 & 44 & 0 \\ 0 & 0 & 80 \end{smallmatrix}\right] \mathrm{nm}$, which we used instead of Eqn. (3). The phasing (location of the minima) of each looping topology was identical to that of the anisotropic model, again, reinforcing the idea that geometry, not choice of elasticity model, sets the phasing. On the other hand, the magnitude of oscillations for the isotropic model were roughly twice those of the anisotropic model for each topology. The isotropic model also predicts nearly identical contributions of individual topologies to the overall looping J factor; or, more precisely, the values of $-\log J$ at each minimum for the four topologies are nearly identical to those predicted from the anisotropic model.

S8.2. Homogeneous elastic model of Czapla et al.

For completeness, we briefly mention another elastic model mentioned in Ref. [26]. Although that work mainly used an elastic model with sequence-dependence, at one point the authors also proposed a simplified model similar to ours. This model posits interspersed "X-" and "Z-"tracts. In our notation, the elastic matrix for "Z-"tracts was taken to be

$$\mathsf{Q}_{\mathrm{Czapla}} = (0.34\,\mathrm{nm}) \left(\frac{180}{\pi}\right)^2 \times \begin{bmatrix} 4.84^{-2} & 0 & 0 \\ 0 & 4.84^{-2} & 5.41^{-2} \\ 0 & 5.41^{-2} & 4.09^{-2} \end{bmatrix} \tag{S11}$$

The elastic matrix for "X-"tracts is the same without the off-diagonal terms.

Although Eqn. (S11) is similar in structure to our Eqn. (3), we note parenthetically that when we use it to calculate the persistence length for the Z-tracts, via the method outlined in Sect. 3.3, we obtain $33\,\mathrm{nm}$, which is much too small. We instead used the elasticity theory defined by Eqn. (3) in the present work.

S9. Cyclization

To check that our Monte Carlo algorithm was working properly, and that our mathematical definitions of J etc. were correct, we also computed the cyclization J factor and compared to the classic analytical result of Shimada and Yamakawa [27]. To do the calculation, we modified our boundary conditions to require that, for a DNA conformation to be considered "looped," its ends must coincide and have identical orientations. There is no binding degeneracy, and hence only one loop type (although as mentioned in the text, that type consists of various topoisomers). We used the isotropic elasticity model of Sect. S8.1 because that was

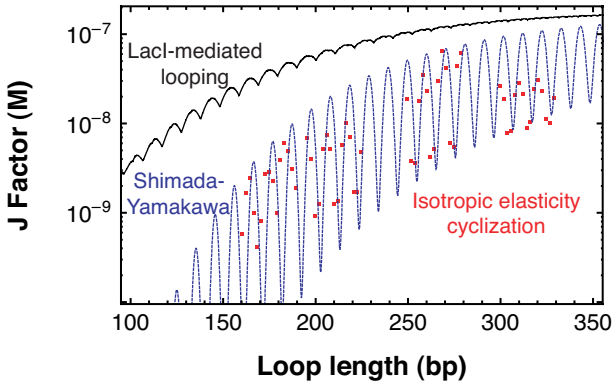

Figure S4. *Red dots:* Cyclization J factor, computed with an isotropic elasticity model. *Blue dashed line:* Analytic calculation of J from Ref. [27], using $\xi = 44$ nm and twist persistence $= 80$ nm. For comparison, the *black line* shows our result for the overall looping J factor (identical to the black line in Fig. 9).

the model used by Shimada and Yamakawa, and we substituted the corresponding values of bend and twist stiffness into their formula, yielding Fig. S4. The figure shows an absolute comparison; no arbitrary rescaling or shifting was done to bring the graphs into agreement. Thus although the mathematical approach and approximations made in [27] are quite different from ours, the calculations are in rough agreement over range of loop lengths that we study.

Comparing cyclization to LacI-mediated looping, we see that for each value of interoperator spacing the looping J factor is larger, particularly at short $L_{\rm loop}$. This difference reflects the lower elastic strain energy for the looping boundary conditions. We also note that adding the four looping topologies largely cancels the periodic modulation in the looping J factor; no such cancellation can occur in the cyclization case.

References

[1] L. Han, H. G. Garcia, S. Blumberg, K. B. Towles, J. F. Beausang, P. C. Nelson, and R. Phillips. Concentration and length dependence of DNA looping in transcriptional regulation. Submitted, 2008.

[2] L. Han, B. H. Lui, S. Blumberg, J. F. Beausang, P. C. Nelson, and R. Phillips. Calibration of tethered particle motion experiments. In C.J. Benham et al., editor, *Mathematics of DNA Structure, Function and Interactions*. Springer, New York, 2008. In press.

[3] P. C. Nelson, C. Zurla, D. Brogioli, J. F. Beausang, L. Finzi, and D. Dunlap. Tethered particle motion as a diagnostic of DNA tether length. *J. Phys. Chem. B*, 110(34):17260–17267, 2006.

[4] L. Finzi and J. Gelles. Measurement of lactose repressor-mediated loop formation and breakdown in single DNA-molecules. *Science*, 267(5196):378–380, 1995.

[5] J. F. Beausang, C. Zurla, L. Finzi, L. Sullivan, and P.C. Nelson. Elementary simulation of tethered Brownian motion. *Am. J. Phys.*, 75:520–523, 2007.

[6] J. F. Beausang, C. Zurla, C. Manzo, D. Dunlap, L. Finzi, and P. C. Nelson. DNA looping kinetics analyzed using diffusive hidden Markov model. *Biophys. J.*, 92:L64–L66, 2007.

[7] J. F. Beausang and P. C. Nelson. Diffusive hidden Markov model characterization of DNA looping dynamics in tethered particle experiments. *Phys. Biol.*, 4:205–219, 2007.

[8] X.-J. Lu and W. K. Olson. 3DNA: A software package for the analysis, rebuilding and visualization of three-dimensional nucleic acid structures. *Nucl. Acids Res.*, 31(17):5108–5121, 2003.

[9] M. Lewis. The lac repressor. *C. R. Biologies*, 328:521–548, 2005.

[10] L. Bintu, N. E Buchler, H. G. Garcia, U. Gerland, T. Hwa, J. Kondev, and R. Phillips. Transcriptional regulation by the numbers: Models. *Curr. Op. Genetics Devel.*, 15:116–124, 2005.

[11] L Bintu, NE Buchler, HG Garcia, U Gerland, T Hwa, J Kondev, T Kuhlman, and R Phillips. Transcriptional regulation by the numbers: Applications. *Curr. Op. Genetics Devel.*, 15(2):125–135, 2005.

[12] L. Saiz, J. M. Rubi, and J. M. Vilar. Inferring the in vivo looping properties of DNA. *Proc. Natl. Acad. Sci. USA*, 49:17642–17645, 2005.

[13] F. Vanzi, C. Broggio, L. Sacconi, and F. S. Pavone. Lac repressor hinge flexibility and DNA looping: Single molecule kinetics by tethered particle motion. *Nucl. Acids Res.*, 34(12):3409–3420, 2006.

[14] O. V. Tsodikov, R. M. Saecker, S. E. Melcher, M. M. Levandoski, D. E. Frank, M. W. Capp, and M. T. Record. Wrapping of flanking non-operator DNA in lac repressor-operator complexes: Implications for DNA looping. *J. Mol. Biol.*, 294(3):639–655, 1999.

[15] O. K. Wong, M. Guthold, D. A. Erie, and J. Gelles. Interconvertible lactose repressor–DNA looped complexes revealed by single-molecule experiments. *PLoS Biology*, 6:e232–(1–15), 2008.

[16] C.M. Falcon and K.S. Matthews. Glycine insertion in the hinge region of lactose repressor protein alters DNA binding. *J. Biol. Chem.*, 274:30849–30857, 1999.

[17] A. M. Friedman, T. O. Fischmann, and T. A. Steitz. Crystal structure of lac repressor core tetramer and its implications for DNA looping. *Science*, 268(5218):1721–1727, 1995.

[18] G. C. Ruben and T. B. Roos. Conformation of Lac repressor tetramer in solution, bound and unbound to operator DNA. *Microsc. Res. Tech.*, 36(5):400–416, 1997.

[19] L. M. Edelman, R. Cheong, and J. D. Kahn. Fluorescence resonance energy transfer over $\sim$130 basepairs in hyperstable lac repressor-DNA loops. *Biophys. J.*, 84:1131–1145, 2003.

[20] D Normanno, F Vanzi, and FS Pavone. Single-molecule manipulation reveals supercoiling-dependent modulation of *lac* repressor-mediated DNA looping. *Nucl. Acids Res.*, 36:2505–2513, 2008.

[21] Y. Zhang, A.E. McEwen, D.M. Crothers, and S.D. Levene. Analysis of in-vivo LacR-mediated gene repression based on the mechanics of DNA looping. *PLoS ONE*, 1(1):e136–(1–13), 2006.

[22] D. Swigon, B. D. Coleman, and W. K. Olson. Modeling the Lac repressor-operator assembly: The influence of DNA looping on Lac repressor conformation. *Proc. Natl. Acad. Sci. USA*, 103(26):9879–9884, 2006.

[23] E. Villa, A. Balaeff, and K. Schulten. Structural dynamics of the lac repressor-DNA complex revealed by a multiscale simulation. *Proc. Natl. Acad. Sci. USA*, 102(19):6783–6788, 2005.

[24] J. Muller, S. Oehler, and B. Muller-Hill. Repression of lac promoter as a function of distance, phase and quality of an auxiliary lac operator. *J. Mol. Biol.*, 257(1):21–29, 1996.

[25] Z. Alexandrowicz. Monte Carlo of chains with excluded volume: A way to evade sample attrition. *J. Chem. Phys.*, 51:561–565, 1969.

[26] L. Czapla, D. Swigon, and W. K. Olson. Sequence-dependent effects in the cyclization of short DNA. *J. Chem. Theor. Comp.*, 2(3):685–695, 2006.

[27] J. Shimada and H. Yamakawa. Ring-closure probabilities for twisted wormlike chains – applications to DNA. *Macromolecules*, 17:689–698, 1984.